Structural changes at the triclinic-rhombohedral transition and their influence on the Li mobility of the fast-ion conductor $LiHf_2(PO_4)_3$

Miguel A. París and Jesús Sanz
Instituto de Ciencia de Materiales de Madrid, Consejo Superior de Investigaciones Científicas (CSIC), 28049 Cantoblanco, Madrid, Spain
(Received 12 August 1999)

Structural changes produced at the triclinic-rhombohedral transition of $LiHf_2(PO_4)_3$ have been analyzed by NMR spectroscopy: the reduction of symmetry produces differentiation of three tetrahedra PO_4, whose distortions correlate well with chemical shift anisotropies determined by ^{31}P NMR. At the phase transition, ^{31}P chemical shift values change according to the modification of the P-O-Hf angles determined by neutron diffraction data. On the other hand, in the triclinic (low-temperature) phase, the location of lithium along the conduction channels, at midway positions between M_1 and M_2 sites, was confirmed by ^7Li NMR spectroscopy. In these positions, a distorted almost planar fourfold coordination, with Li-O distances near 2.1 Å, explains the observed ^7Li quadrupole coupling constants. In the rhombohedral (high-temperature) phase, the structural changes destabilize lithium coordination. In this case, ^7Li NMR spectra show important lithium mobility and spectral features are intermediate between those of M_1, M_2, and midway sites. The important delocalization of lithium explains the strong increase on conductivity detected at the phase transition that makes this compound one of the best reported lithium ion conductors.

I. INTRODUCTION

Lithium ion conducting solids is a topic of great interest because of their potential application as electrolytes in lithium batteries. In particular, lithium compounds with NASICON (Na superionic conductors) structure and formula $LiM_2^{IV}(PO_4)_3$ have been extensively studied for their good ionic conductivity.[1–14] The ideal framework of NASICON-type materials[15–17] is rhombohedral with space group $R\bar{3}c$ and is built up by $M_2(PO_4)_3$ units [Fig. 1(a)]. A pair of MO_6 octahedra is arranged with opposite triangular faces approximately parallel to each other and oriented perpendicularly to the c axis of the structure. Three PO_4 tetrahedra, which have one edge approximately parallel to the c axis, bridge the parallel faces of the two octahedra of $M_2(PO_4)_3$ units. Tetrahedral oxygens involved in edges oriented perpendicularly to the c axis, form part of octahedra of two adjacent units. In the NASICON structure, lithium can occupy two different sites: (i) M_1 sites, surrounded by six oxygens and located at inversion centers and (ii) M_2 sites, with an irregular tenfold oxygen coordination and disposed symmetrically around the threefold axis of the structure. Both sites have different multiplicity (1:3) and alternate along the conduction channels, forming a three-dimensional network [Fig. 1(b)].

$LiM_2^{IV}(PO_4)_3$ compounds with the largest tetravalent cations (M^{IV} = Sn, Hf, Zr) exhibit at low temperatures a structural phase transition[18–21] which causes a distortion of the framework, without breaking bonds. The symmetry of the low-temperature phase of these compounds have been unclear for several years, but it has been established recently to be triclinic.[20–24] In particular, $LiHf_2(PO_4)_3$, one of the compounds of this family with higher conductivity values, exhibits the structural phase transition around 0 °C. The lattice symmetry of the low-temperature phase was deduced by ^{31}P NMR and XRD techniques,[20] however, some doubts remained about lithium location in the triclinic phase. From NMR data, lithium occupation of M_1 sites was clearly rejected and first calculations of quadrupole constants for M_2 sites, carried out using atomic coordinates of the rhombohedral phase, gave values (C_Q = 118 kHz) comparable to the experimental one (C_Q = 180 kHz).[25] On these bases, it was suggested that lithium could occupy M_2 sites in the triclinic phase. In the mean time, the crystallographic structure of both phases has been solved[22] by neutron diffraction. In the triclinic phase, lithium ions were located at intermediate positions between M_1 and M_2 sites; however, lithium location could not be deduced with reliability in the rhombohedral phase. In the present work we are going to analyze the structural changes produced during the phase transition and to correlate them with the variations observed in ^{31}P and ^7Li NMR spectra.

II. EXPERIMENT

The sample was prepared by calcination of a stoichiometric mixture of Li_2O, $(NH_4)_2H(PO_4)_3$ and HfO_2 at increas-

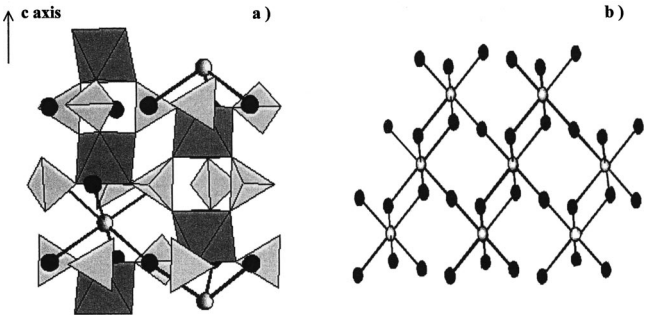

FIG. 1. Schematic view of (a) the NASICON framework, where the basic units $M_2(PO_4)_3$, formed by two octahedra MO_6 and three tetrahedra PO_4, can be identified. (b) conduction channels connecting M_1 (white circles) and M_2 (black circles) sites.

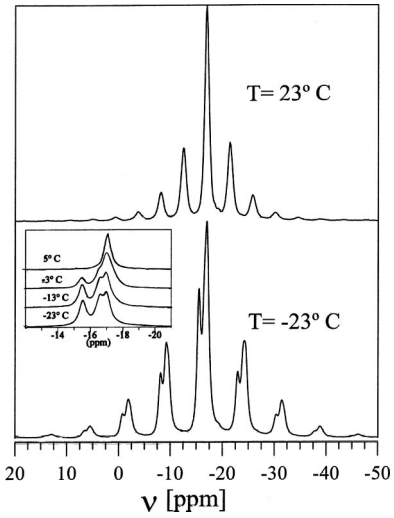

FIG. 2. MAS ^{31}P NMR spectra recorded at $T=23$ and -23 °C. In the insets of the figure, the central component of these spectra are displayed.

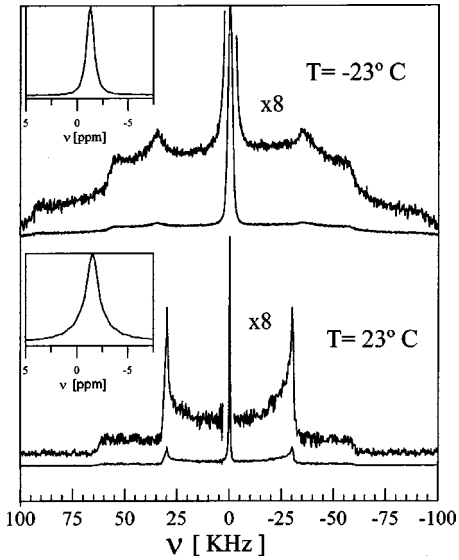

FIG. 3. Static ^{7}Li NMR spectra recorded at $T=23$ and -23 °C. To highlight the pattern of the satellite transitions, the scale of the y axis has been multiplied by the indicated factors. In the insets of the figure, the central component of the MAS ^{7}Li NMR spectra, recorded at the same tempe rature, are displayed.

ing temperatures in the range 850–1100 °C. A more detailed description of the sample preparation is reported elsewhere.[13]

^{31}P and ^{7}Li NMR spectra, recorded in static and MAS conditions, were obtained at different temperatures between 22 and -43 °C by using a B-VT 1000/SU07 unit in a MSL 400 Bruker spectrometer. The frequencies used for ^{31}P and ^{7}Li spectra were 161.96 and 155.45 MHz. Spectra were taken after $\pi/2$ pulse irradiation. A time interval between successive scans in the range 2–30 sec was chosen, depending on the spin-lattice relaxation times of the two nuclei at each temperature. The number of accumulations was in the range 10–200. The ^{7}Li and ^{31}P chemical shift values are given relative to 1 M LiCl and 85% H_3PO_4 aqueous solutions, respectively. The fitting of NMR spectra was carried out with the Bruker WINFIT program,[26] which computes the intensities of the spinning sidebands with the Herzfeld and Berger method.[27] With this program, the spinning rate and the position, linewidth and intensity of the components were determined with a standard nonlinear least square method. However, the anisotropy and asymmetry parameters, which characterize nuclear interactions, have to be determined by a trial and error procedure. Once, the experimental envelope was fitted, the sum of intensities of sidebands of components was calculated by numerical integration.

III. RESULTS

A. ^{31}P NMR

The ^{31}P MAS NMR spectrum of the compound $LiHf_2(PO_4)_3$, recorded at -23 °C, is shown in Fig. 2. Three central lines and their corresponding spinning sidebands, spaced at ~6 ppm (spinning rate expressed in ppm), are observed. As the chemical environment of all phosphorus atoms is the same, $P(OHf)_4$, the observed components correspond to three nonequivalent crystallographic sites. Integration of the sidebands of the three components, according to the procedure described in the experimental section, gave intensities proportional to 1:1:1, indicating that the three sites have the same multiplicity. The intensity of the three central lines detected at -23 °C decreases during sample heating (around 0 °C) and a new line, with the same position that one of previous components, is detected (inset of Fig. 2). At room temperature, the ^{31}P MAS spectrum displays the single component, characteristic of the rhombohedral symmetry (one crystallographic site).

From analysis of the spinning side bands pattern of ^{31}P MAS-NMR spectra, the isotropic chemical shift (σ_{iso}),

TABLE I. Chemical shift tensor values (σ_{iso}, $\Delta\sigma$, η_{cs}) and quadrupole coupling parameters (C_Q, η_Q) deduced from fitting of ^{31}P and ^{7}Li NMR spectra, respectively.

	^{31}P			^{7}Li	
	σ_{iso} [ppm]	$\Delta\sigma$ [ppm]	η_{cs}	C_Q [kHz]	η_Q
Rhombohedral	-17.1 ± 0.1	-8 ± 1	1	118 ± 6	0
Triclinic	-15.5 ± 0.1	16 ± 1	0.95 ± 0.05	180 ± 6	0.30 ± 0.03
	-16.5 ± 0.1	18 ± 2	0.95 ± 0.05		
	-17.0 ± 0.1	13 ± 3	0.95 ± 0.05		

TABLE II. Structural parameters of HfO_6 octahedra in the two phases of $LiHf_2(PO_4)_3$.

		Triclinic					
	Rhombohedral		Hf1			Hf2	
Hf-O1 (Å)	3×2.03	2.01	2.03	2.04	2.04	2.12	2.14
Hf-O2 (Å)	3×2.07	2.05	2.07	2.14	2.02	2.03	2.04
O1-O1 (Å)	3×2.91	2.87	2.90	2.95	2.89	2.89	2.92
O2-O2 (Å)	3×2.81	2.69	2.82	2.88	2.98	2.98	3.06
O1-Hf-O1 (°)	3×91.7	90.4	91.2	93.3	85.7	88.1	88.7
O2-Hf-O2 (°)	3×85.7	79.1	86.4	86.8	94.3	94.3	97.3
O1-Hf-O2 (°)	3×89.0	88.3	88.6	96.9	84.9	89.7	89.9
O1-Hf-O2 (°)	3×93.5	91.4	93.3	93.4	87.0	87.4	91.7
β_1 (°)	0		7.2			7.8	
β_2 (°)	0		4.3			5.9	

the anisotropy ($\Delta\sigma$), and the asymmetry parameter (η_{cs}) of P environments were determined in two phases (see Table I).

B. ^{7}Li NMR

^{7}Li($I=\frac{3}{2}$) static NMR spectra, obtained at room temperature and -23 °C, are plotted in Fig. 3. A central line and two satellite transitions form both spectra. The experimental second moment $\Delta\varpi^2$ of the central line deduced from the spectrum obtained at low temperatures is $0.36\pm0.03\,G^2$. The linewidth of the central transition ($-\frac{1}{2}\rightarrow\frac{1}{2}$ transition) narrows and its line shape changes from Gaussian to Lorentzian when going from the spectrum obtained at -23 °C to the room-temperature one. This fact is due to the strong increase on the lithium mobility detected by conductivity and ^{7}Li NMR techniques around the phase transition temperature[20] (motional line narrowing).

On the other hand, the broad symmetric pattern ($\frac{1}{2}\rightarrow\frac{3}{2}$, $-\frac{3}{2}\rightarrow-\frac{1}{2}$ satellite transitions) is caused by the interaction of the quadrupole moment of nuclei with the electric field gradient at structural sites.[28] It can be seen that the quadrupole pattern of the low-temperature spectrum is different and covers a wider frequency range than that of the room-temperature spectrum (Fig. 3 top and bottom). From analysis of both spectra, determination of the quadrupole coupling constants, C_Q, and the asymmetry parameters, η_Q, have been done (Table I).

In order to study lithium location, ^{7}Li MAS-NMR spectra, recorded at the same temperatures than the static ones, have been analyzed (insets of Fig. 3). In the low-temperature phase, detection of a narrow central line at -1 ppm indicates that lithium occupies only one type of site. In the rhombohedral phase, the NMR line shifts to -1.7 ppm, indicating that Li changes its location. The increase of the linewidth of the central component with temperature suggests the existence of exchange processes between different structural sites.

IV. DISCUSSION

A. Structural changes of the NASICON framework

Atomic positions determined from the neutron diffraction study[22] have been used to analyze the structural changes produced at the phase transition. For that, we have described the triclinic lattice in terms of a pseudorhombohedral coordinate system, at which the pseudoternary axis of the structure coincides with the $(103)_T$ triclinic direction. In this analysis, it has been considered the effect of the reduction of symmetry on the number of independent crystallographic positions. Thus, for instance, the two oxygens of the rhombohedral phase (O_1 and O_2) give 12 different types of oxygens in the triclinic phase.

In Table II the geometry and relative orientation of octahedra HfO_6 are given. It can be seen that significant modifications are produced in the internal geometry of octahedra (distances Hf-O, O-O, and angles O-Hf-O) during the phase transition. In the rhombohedral phase, these octahedra can be considered as constituted by two equilateral triangles, normal to the ternary axis, with edges almost parallel each other. From Table II, it can be seen that the equilateral triangles become scalene and the O-Hf-O bonds angles change in the triclinic phase. However, the most significant change observed concern the inclination of octahedra with respect to the pseudoternary axis. In particular, the inclination of the two bases of octahedra are different (β_1 and β_2 angles) in the triclinic phase.

Now we will analyze the modifications produced at tetrahedra PO_4. It can be seen (Table III) that modifications produced in the internal geometry of tetrahedra (distances P-O and angles O-P-O) are less important that in octahedra. However, a significant change is observed in angles which define the orientation of tetrahedra, i.e., the angle subtended by the O_1-O_1 edge, initially parallel to the ternary axis (α_1) and that defined by the O_2-O_2 edge, initially disposed at planes perpendicular to this axis (α_2). These angles are close to zero in the rhombohedral phase and higher in the triclinic phase. In the triclinic phase, the orientation and geometry of the $P1$ and $P2$ tetrahedra are relatively similar each other but different from the $P3$ tetrahedron.

On the other hand, the analysis of the angles Hf-O-P (Table III) shows appreciable modifications on Hf-O1-P angles, constituting basic units, and angles Hf-O2-P, relating adjacent structural units, when going from rhombohedral to triclinic phase. Thus, the internal Hf-O1-P angles constituting the basic lanterns, near 158° in the rhombohedral phase, are spread over a broad range (138°–170°) and the external Hf-O2-P angles, near 142° in the rhombohedral phase, are dispersed over 133°–160° in the triclinic phase.

TABLE III. Structural parameters of PO_4 tetrahedra in the two phases of $LiHf_2(PO_4)_3$.

	Rhombohedral	Triclinic $P1$		$P2$		$P3$	
P-O1 (Å)	2×1.51	1.51	1.59	1.49	1.56	1.52	1.53
P-O2 (Å)	2×1.54	1.51	1.55	1.51	1.56	1.49	1.53
O1-P-O1 (°)	110.7	108.5		111.5		109.4	
O2-P-O2 (°)	108.0	110.0		109.9		112.8	
O1-P-O2 (°)	2×107.5	107.2	110.2	105.2	111.3	103.1	107.3
O1-P-O2 (°)	2×111.6	109.7	111.1	109	109.8	111.0	113.2
α_1 (°)	3.6	12.3		8.6		20.7	
α_2 (°)	−0.8	4.7		5.0		15.4	
Hf-O1-P (°)	2×158.2	142.0	161.2	140.8	170.4	138.1	154.2
Hf-O2-P (°)	2×142.3	132.8	149.1	143.6	145.7	152.9	160.1

Although structural changes produced in the Nasicon's framework are not very large, they are significant enough to be analyzed by NMR. In first approximation, in $LiM_2^{IV}(PO_4)_3$ compounds, the isotropic chemical shift (σ_{iso}) of ^{31}P signal is given by the polarizing strength of the M^{IV} cation.[25] However, for a given compound, σ_{iso} depend on the relative disposition of contiguous polyhedra. An empirical relation frequently used to explain chemical shift values is[29]

$$\sigma_{iso} = -A \times \left\langle \frac{\cos\theta_{P\text{-}O\text{-}Hf}}{\cos\theta_{P\text{-}O\text{-}Hf} - 1} \right\rangle + B, \quad (1)$$

where A is positive and the angular brackets stand for the average value of the four angles P-O-Hf, that relates contiguous polyhedra. On the other hand, the absolute value of the chemical shift anisotropy ($|\Delta\sigma|$) can be related to tetrahedra distortions through the expression[30]

$$|\Delta\sigma| = A \times \frac{\sum_{i=1}^{4} |\ln(l_i/l_o)|}{4} + B, \quad (2)$$

where, again, A is positive, l_i are the distances P-O and $l_o = 1.545$ Å is the distance P-O for a regular tetrahedron. In Table IV it is shown that the predictions obtained with these expressions explain most of experimental observations in the two phases of $LiHf_2(PO_4)_3$.

From the whole analysis it can be concluded that the phase transition produces distortions on polyhedra and affects considerably their relative disposition in the NASICON framework. This effect is visualised in Fig. 4 and will be important to explain the lithium location.

B. Lithium location

Lithium atoms can occupy different positions in the NASICON framework (M_1, M_2, and midway sites), however, little information can be obtained by x-ray diffraction about this point. On the other hand, $LiGe_2(PO_4)_3$,[31] $LiTi_2(PO_4)_3$,[32] $LiSn_2(PO_4)_3$,[33] $LiZr_2(PO_4)_3$,[34] and $LiHf_2(PO_4)_3$ (Ref. 22) compounds have been studied by neutron diffraction. From the study of the rhombohedral compounds a preferential occupation of M_1 sites was deduced in M^{IV}=Ge and Ti, however, in the triclinic phases of $LiHf_2(PO_4)_3$, $LiZr_2(PO_4)_3$, and $LiSn_2(PO_4)_3$, midway sites M_1/M_2 (hatched circles in Fig. 4) seem to be occupied. ^7Li NMR spectroscopy was used in a previous work[25] to analyze structural characteristics of sites occupied by lithium. In particular, in the rhombohedral compounds occupation of M_1 sites was deduced, however, in the triclinic phases some doubts remained concerning the type of sites occupied by lithium. In the present work, structural data obtained recently on the triclinic phase of $LiHf_2(PO_4)_3$ will allow us to clarify this point.

1. Analysis of the second moment ($\Delta\varpi^2$)

In the triclinic phase of $LiHf_2(PO_4)_3$, the ^7Li static NMR spectrum recorded at −23 °C can be fitted with a unique quadrupole pattern and the central component of the ^7Li MAS-NMR spectrum is formed by a single narrow line. Both observations suggest that lithium occupies a unique site in the triclinic phase of $LiHf_2(PO_4)_3$.

If it is assumed that the broadening of the central line of ^7Li NMR spectra is mainly due to dipole interactions, an

TABLE IV. Correlation between the structural parameters of PO_4 tetrahedra and chemical-shift tensor values deduced from ^{31}P MAS-NMR spectra. See expressions (1) and (2) of the text for details.

	Rhombohedral	Triclinic $P1$	$P2$	$P3$
$\left\langle \frac{\cos\theta_{P\text{-}O\text{-}Hf}}{\cos\theta_{P\text{-}O\text{-}Hf}-1} \right\rangle$	0.461	0.448	0.458	0.464
$\frac{\sum_{i=1}^{4}\lvert\ln(l_i/l_o)\rvert}{4}$	0.011	0.020	0.017	0.016
σ_{iso} [ppm]	−17.1±0.1	−15.5±0.1	−16.5±0.1	−17.0±0.1
$\Delta\sigma$ [ppm]	−8±1	16±1	18±2	13±3

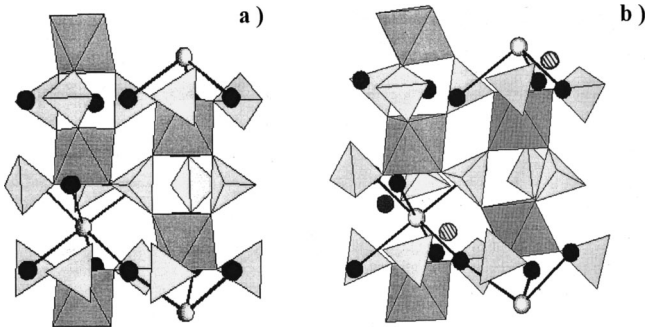

FIG. 4. Structure of the rhombohedral (a) and triclinic (b) phases of $LiHf_2(PO_4)_3$. In these structures, the orientation of octahedra and tetrahedra are clearly different. In the triclinic phase, hatched circles correspond to midway sites occupied by lithium, and white and black circles are M_1 and M_2 sites.

analysis of the linewidth can be used to deduce the positions occupied by lithium in the triclinic phase (in absence of ionic mobility). For that, the second moment ($\Delta\varpi^2$) of the central transition of the spectrum, recorded at low temperature in static conditions, has been compared with values calculated for the different positions of lithium in the Nasicon structure, by using the Van Vleck's expression for a rigid lattice;[35]

$$\Delta\varpi^2=\frac{3}{5}\gamma_I^4\hbar^2 I(I+1)\sum_k \frac{1}{r_{jk}^6}+\frac{4}{15}\gamma_I^2\gamma_S^2\hbar^2 S(S+1)\sum_k \frac{1}{r_{jk}^6}. \tag{3}$$

The first term accounts for dipole interactions between like spins and the second one for unlike spins. γ_I and γ_S are the gyromagnetic ratios for I and S spins and r_{jk} is the distance between interacting spins. The sum on k extends over all nuclei that interact with the reference nucleus j.

A comparison of the experimental value of $\Delta\varpi^2$ and the calculated ones is given in Table V. It can be seen that Li-P dipole interaction is much more important than Li-Li interaction, whatever site lithium occupies. The calculated values for the two nonequivalent M_1 sites of the triclinic phase are much lower than the experimental one. However, the calculated values for the three nonequivalent M_2 sites and for the midway M_1-M_2 site deduced from neutron diffraction data[22] are similar each other and closer to the experimental one.

TABLE V. Calculated second moment ($\Delta\varpi^2$) corresponding to lithium occupying different structural sites of the triclinic $LiHf_2(PO_4)_3$ phase. The experimental value was deduced from the central transition of the ^{7}Li NMR static spectrum.

	Calculated			Experimental
Site	$\Delta\varpi^2_{\text{Li-P}}$ [G^2]	$\Delta\varpi^2_{\text{Li-Li}}$ [G^2]	$\Delta\varpi^2_{\text{cal}}$ [G^2]	$\Delta\varpi^2$ [G^2]
M_1a (1/4–1/4 0)	0.06	0.03	0.09	
M_1b (1/4 1/4 1/2)	0.07	0.03	0.10	
M_2a (1/2 0.95 1/4)	0.22	0.06	0.28	0.36±0.03
M_2b (0.83 0.1 0.7)	0.19	0.08	0.27	
M_2c (0.83 −0.1 0.2)	0.19	0.08	0.27	
midway M_1/M_2 (0.11 0.347 0.419)	0.16	0.08	0.24	

Based on this fact, the analysis of $\Delta\varpi^2$ values cannot discriminate by itself on the lithium occupation of these two sites.

2. Analysis of the quadrupole coupling parameters (C_Q and η_Q)

Another way to analyze structural positions occupied by lithium concerns the study of the quadrupole coupling parameters C_Q and η_Q (Ref. 28)

$$C_Q=\frac{e^2QV_{zz}}{h},\quad \eta_Q=\frac{V_{xx}-V_{yy}}{V_{zz}}, \tag{4}$$

where Q is the quadrupole moment of nuclei and V_{xx}, V_{yy}, and V_{zz}, are the principal values of the electric field gradient (EFG) tensor at the position of the nuclei. The criterion followed to label the principal axes is

$$|V_{zz}|\geqslant|V_{yy}|\geqslant|V_{xx}|. \tag{5}$$

C_Q measures the deviation of the structural environment from the cubic symmetry and η_Q, the deviation from the axial symmetry.

Assuming that compounds are predominantly ionic, the components of the EFG tensor can be calculated on the basis of a point charge model through the expression

$$V_{ij}=\frac{1}{4\pi\varepsilon_0}\sum_k eZ_k\frac{3x_i^kx_j^k-r_k^2\delta_{ij}}{r_k^5}, \tag{6}$$

where eZ_k is the electric charge of the kth ion. The principal components of the EFG tensor are obtained by diagonalizing the matrix V_{ij}, and C_Q and η_Q with Eqs. (4). Although η_Q can be calculated directly from the EFG tensor, calculation of C_Q requires an estimate of the Sternheimer shielding γ_∞ factor[36,37] [$C_Q=e^2Q(1-\gamma_\infty)V_{zz}/h$], which accounts for distortions induced in the core electrons of the ion by the quadrupole field of the nucleus and by the external field gradients. For Li^+, γ_∞ can be assumed to be 0.3.[25,38,39] The summation indicated in Eq. (6) is performed numerically in a Cartesian coordinate system. It was found that convergence in V_{ij} calculations, with errors less than 2%, can be obtained if all ions within a radius of 30 Å are considered.

The EFG tensor can be expressed as a sum of the contributions corresponding to each sublattice:

$$V_{ij}=Z_{\text{Li}}V_{ij}^{\text{Li}}+Z_{\text{Hf}}V_{ij}^{\text{Hf}}+Z_{\text{P}}V_{ij}^{\text{P}}+Z_{\text{O}}V_{ij}^{\text{O}}. \tag{7}$$

On these bases, the EFG tensor was calculated for the three types of sites available for lithium in the triclinic phase of $LiHf_2(PO_4)_3$ (M_1, M_2, and midway M_1/M_2). In general, $\overline{\overline{V}}$ is not diagonal, therefore, diagonalization of $\overline{\overline{V}}$ tensor was a previous step to evaluate the principal components for each charge set considered. C_Q values obtained using nominal charges values are, for all the positions, much higher than the experimental one, indicating that the structural framework has a partial covalent character and that a net reduction of the atoms charge is produced.

In order to calculate more realistic C_Q values, two assumptions were made: first, a fully ionized lithium is considered ($Z_{\text{Li}}=+1$) and, secondly, the effective charges for all types of oxygen are assumed to be equal. Both suppositions

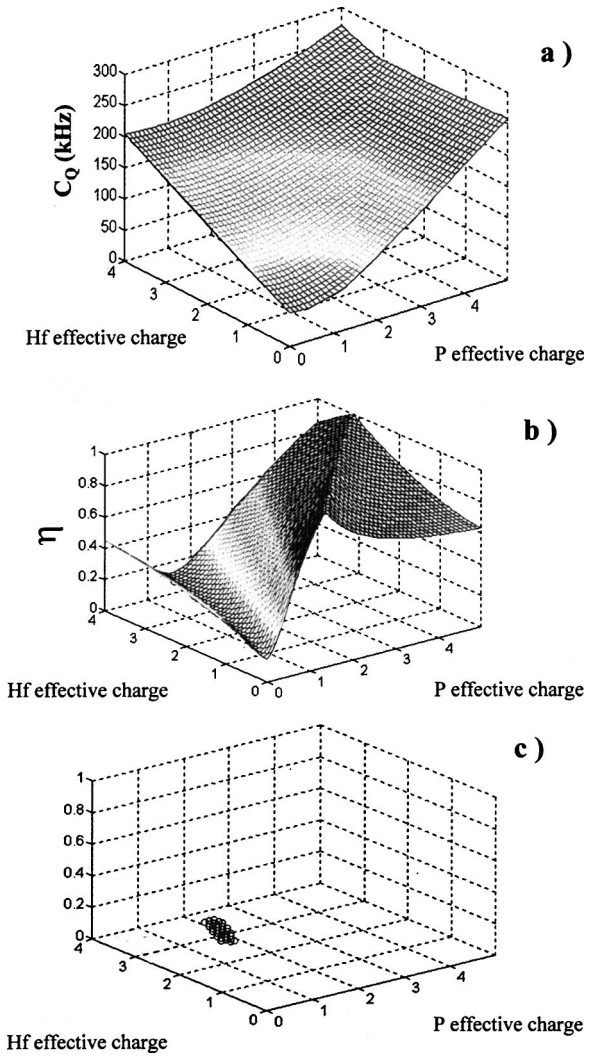

FIG. 5. Dependence of the calculated (a) C_Q and (b) η values on the effective charge of P and Hf atoms for the midway M_1-M_2 site in the triclinic phase of $LiHf_2(PO_4)_3$. (c) Charge values that reproduce experimental C_Q and η values.

seem to be reasonable and not very restrictive in our analysis. Taking into account these hypotheses and the condition of electrical neutrality, the only free parameters are Z_{Hf} and Z_p in Eq. (7). An analysis of C_Q and η_Q values as a function of the charge assigned to hafnium and phosphorus atoms showed that only the localization of lithium at the midway position M_1/M_2 reproduce experimental values with charge values having physical meaning. Moreover, these charge values ($2<Z_P<2.5$ and $2.5<Z_{hf}<3.5$) are very close to those deduced in previous calculations[25] for the rhombohedral $LiGe_2(PO_4)_3$ and $LiTi_2(PO_4)_3$ compounds. In Fig. 5, a plot of C_Q and η_Q values, calculated for midway M_1-M_2 sites as a function of the effective charge assigned to Hf and P, is given. In the same figure, it is also shown the region that fit simultaneously experimental C_Q and η_Q values. Taking the charge values deduced, the quadrupole coupling parameters associated with M_1 and M_2 sites were also estimated (Table VI). It can be seen that the three M_2 sites have C_Q values higher than those deduced for M_1 sites, but still lower than that deduced for midway M_1/M_2 sites. On the contrary, η value of the midway M_1/M_2 sites is lower than M_2 sites and much lower than value of M_1 sites.

3. Lithium coordination and its relationship to mobility

In order to understand the preferential occupation of midway M_1/M_2 sites in the triclinic phase, we have analyzed the lithium coordination, i.e., the distances Li-O for all the possible sites in this structure (Table VII). From this analysis, it can be seen that in the midway M_1-M_2 sites, lithium exhibits a compact almost planar fourfold coordination with distances Li-O close to 2.10 Å, that are near to the sum of ionic radii of lithium and oxygen atoms, Fig. 6. On the contrary, lithium at M_1 sites is surrounded by a quite open octahedral cavity with Li-O distances ranging from 2.5 to 2.9 Å. In a similar way, lithium environment at M_2 sites is a quite open tenfold coordination with very different distances (2.1 to 3.4 Å). These facts suggest that lithium is better stabilized in the midway M_1-M_2 sites of the triclinic phase of $LiHf_2(PO_4)_3$. Similar conclusions have been recently deduced from the neutron diffraction analysis of the triclinic $LiSn_2(PO_4)_3$ (Ref. 33) and $LiZr_2(PO_4)_3$ (Ref. 34) phases.

In Table VII the Li-O distances are also given for the three sites in the rhombohedral phase. In particular, it is observed that average Li-O distances have appreciably increased for midway M_1-M_2 sites from 2.10 to 2.27 Å, making lithium coordination uncomfortable in this position. On the other hand, as distances Li-O are still quite large for M_1 and M_2 sites (larger than 2.40 Å), lithium cannot be effectively coordinated in either of these two sites. From these considerations, it is evident that lithium mobility must be favored in the rhombohedral phase.

On the other hand, it has been proposed the existence of two triangular bottlenecks, relating M_1 and M_2 sites, that limit lithium mobility in NASICON compounds.[40–42] In particular, it was suggested that oxygens of triangles $T_1(O_2O_2O_1)$ and $T_2(O_2O_2O_2)$, see Fig. 6, are bottlenecks that limit lithium diffusion in conduction channels $\cdots M_1$-M_2-$M_1\cdots$. An analysis of the geometry of these windows in the two phases of $LiHf_2(PO_4)_3$ has shown that in the triclinic phase, triangles $T2$ are formed by sides with lengths of 2.69, 4.12, and 4.33 Å but $T1$ windows must be considered four-sided poligones, with distances 2.69, 3.28, 3.17, and 2.39 Å. This coordination is produced by the approxi-

TABLE VI. Quadrupole coupling constants C_Q and η_Q, calculated for different structural sites of lithium at the low- and high-symmetry phases of $LiHf_2(PO_4)_3$. Experimental values of each pahse are given for comparison.

	Rhombohedral				Triclinic						
	M_1	M_2	Midway	Exper.	M_1a	M_1b	M_2a	M_2b	M_2c	Midway	Exper.
C_Q (KHz)	25±25	130±20	90±10	118±6	70±10		160±25	90±20	140±20	180±20	180±6
η_Q	0	0.4±0.2	0.1±0.1	0	0.7±0.3		0.52±0.03	0.6±0.4	0.47±0.07	0.30±0.05	0.30±0.03

TABLE VII. Lithium coordination at the possible structural sites for the rhombohedral and triclinic phases of $LiHf_2(PO_4)_3$

	Rhombohedral	Triclinic	
	M_1	M_1a	M_1b
Li-O2 (Å)	6×2.46	2×2.49 2×2.55 2×2.63	2×2.61 2×2.73 2×2.96
	M_2	M_2a	M_2b	m_2c
Li-O2 (Å)	2×2.37	2.21	2.14	2.03
		2.43	2.45	2.68
	2×2.74	2.70	2.90	2.83
		3.27	3.38	3.10
Li-O1 (Å)	2×2.74	2.00	2.33	2.17
		2.60	2.56	2.61
	2×2.77	2.68	2.73	2.83
		2.76	2.77	3.04
	2×2.91	3.00	2.97	3.08
		3.01	3.56	3.11
	Midway		Midway	
Li-O2 (Å)	2.13		2.03	
	2.26		2.29	
	2.47			
Li-O1 (Å)	2.22		1.93	
			2.17	

mation of T_4 tetrahedron to lithium ions (see Fig. 6). In the rhombohedral phase, $T2$ windows have sides with distances 2.81, 4.04, and 4.04 Å and $T1$ windows distances 2.81, 3.78, 3.87, and 2.47 Å. A determination of the radius of the circumscribed spheres in both bottlenecks was done and from that the Li-O distances necessary to pass lithium through the windows estimated. These distances resulted to be 2.08 and 2.21 Å for T_1 and T_2 windows in the triclinic phase and 2.16 and 2.18 Å in the rhombohedral phase. Li-O distances for a fourfold coordination of Li are near 2.00 Å. From this fact, it can be concluded that windows T_1 limit lithium mobility in the triclinic phase, but the slight opening produced during the triclinic-rhombohedral transition eliminates lithium motion hindering, enhancing drastically lithium diffusion.

In order to analyze the lithium location at particular sites of the rhombohedral phase, we have calculated the quadrupole coupling C_Q constants for the three structural sites (Table VI). In all cases, the calculated values differ from the experimental one. As the lithium mobility is important in this phase, an exchange of lithium between different sites must be operating and, therefore, the observed C_Q value should correspond to the average of values of sites occupied by lithium during its movement. On the basis of a fast exchange between M_1, M_2, and midway M_1-M_2 sites, C_Q values would be given by the expression

$$C_Q=\frac{C_Q^1P_1+C_Q^2 3P_2+C_Q^{12}3P_{12}}{P_1+3P_2+3P_{12}}, \tag{8}$$

where P_1, P_2, and P_{12} are the occupation probability of M_1, M_2, and midway M_1-M_2 sites, $C_Q^{(1)}$, $C_Q^{(2)}$, and C_Q^{12}

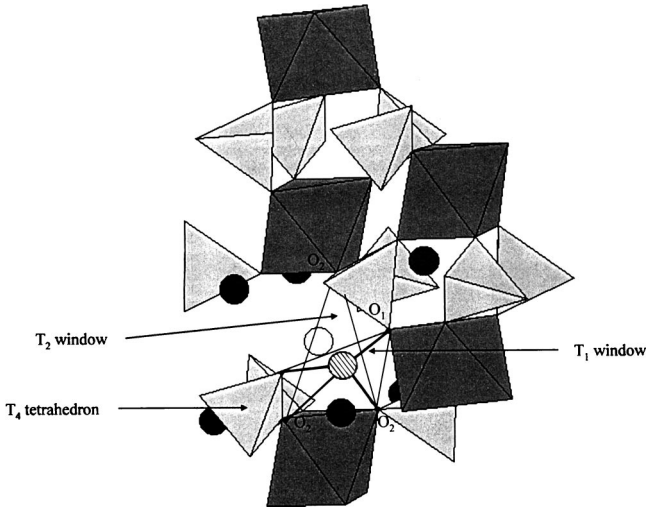

FIG. 6. Schematic view of T_1 and T_2 windows connecting M_1 (white circles) and M_2 (black circles) sites in the triclinic phase of $LiHf_2(PO_4)_3$. Hatched circles correspond to the midway sites occupied by lithium. The solid lines show the lithium coordination in this phase. See the text for a more detailed discussion of the figure.

are the quadrupole coupling constant associated to each site, and the factor 3 takes into account the different multiplicity of structural sites. Assuming a maximum delocalization of lithium ions between all sites ($P_1=P_2=P_{12}=\frac{1}{7}$), the value obtained with expression (8) is $C_Q\approx 100$ kHz, that is quite close to the experimental one (118 kHz). The difference observed between experimental and calculated values could correspond to a slight preference of lithium to reside at M_2 sites in the rhombohedral phase. Moreover, as M_2 and midway sites are disposed symmetrically around the ternary axis of the structure, the fast exchange between these sites gives a η_Q value near zero. The equal occupation of equivalent sites around the ternary axis, produced during lithium motion, is compatible with the ideal rhombohedral $R\bar{3}c$ symmetry of Nasicon compounds, and explains that lithium location was not possible to be deduced by diffraction methods.[22]

V. CONCLUSIONS

In this work, a detailed analysis of the distortions produced at the triclinic-rhombohedral phase transition of $LiHf_2(PO_4)_3$ has been carried out. In particular, it has been shown that the phase transition produces considerable distortions of polyhedra, affecting, without breaking bonds, the relative disposition of tetrahedra PO_4 and octahedra HfO_6 in the NASICON framework.

Moreover, the use of NMR spectroscopy was particularly suitable to study characteristics of the structural sites occupied by lithium in the NASICON structure. Thus, the ^{7}Li NMR study of the triclinic (low temperature) phase of $LiHf_2(PO_4)_3$ has confirmed the positions proposed previously by neutron diffraction for lithium ions, which are located between M_1 and M_2 sites of the NASICON structure. The preference for midway sites compared to M_1 and M_2 positions has been explained on the basis of a much better lithium coordination. In these positions, oxygens constituting

lithium coordination define an irregular almost planar four-sided window that limits severely lithium mobility in the NASICON structure.

In the rhombohedral (high-temperature) phase, structural changes produced in the covalent framework produces an increase on Li-O distances at the midway M_1-M_2 sites that makes uncomfortable lithium coordination. This produces a dramatic increase on the lithium mobility that is responsible for the abrupt increase of ionic conductivity and the strong reduction of the activation energy detected at the phase transition.[20] In the rhombohedral phase, spectral features of the ^{7}Li NMR signal are intermediate between those of the three structural sites. Obtained results have been interpreted on the basis of a fast exchange between three sites, that explains difficulties to localize Li ions in the rhombohedral phase by diffractometric techniques.

ACKNOWLEDGMENTS

We are grateful to Dr. J. M. Rojo and Dr. A. Martínez-Juárez for supplying the analyzed sample and Dr. M. A. Aranda and Dr. S. Bruque for fruitful discussions.

[1] R. D. Shannon, B. E. Taylor, A. D. English, and T. Berzins, Electrochim. Acta **22**, 783 (1977).
[2] B. E. Taylor, A. D. English, and T. Berzins, Mater. Res. Bull. **12**, 171 (1977).
[3] M. A. Subramanian, R. Subramanian, and A. Clearfield, Solid State Ionics **18&19**, 562 (1986).
[4] S. Hamdoune, D. Tran Qui, and E. J. L. Schouller, Solid State Ionics **18&19**, 587 (1986).
[5] S. Li, J. Cai, and Z. Lin, Solid State Ionics **28&30**, 1265 (1988).
[6] B. V. R. Chowdari, K. Radhakrishnan, K. A. Thomas, and G. V. Subba Rao, Mater. Res. Bull. **24**, 221 (1989).
[7] H. Aono, E. Sugimoto, Y. Sadaoka, N. Imanaka, and G. Adachi, J. Electrochem. Soc. **137**, 1023 (1990).
[8] H. Aono, E. Sugimoto, Y. Sadaoka, N. Imanaka, and G. Adachi, Solid State Ionics **47**, 257 (1991).
[9] J. Winand, A. Rulmont, and P. Tarte, J. Solid State Chem. **93**, 341 (1991).
[10] H. Aono, E. Sugimoto, Y. Sadaoka, N. Imanaka, and G. Adachi, J. Electrochem. Soc. **140**, 1827 (1993).
[11] J. Kuwano, N. Sato, M. Kato, and K. Takano, Solid State Ionics **70/71**, 332 (1994).
[12] A. Martínez-Juárez, J. M. Rojo, J. E. Iglesias, and J. Sanz, Chem. Mater. **7**, 1857 (1995).
[13] A. Martínez-Juárez, J. E. Iglesias, and J. M. Rojo, Solid State Ionics **91**, 295 (1996).
[14] M. A. París, A. Martínez-Juárez, J. M. Rojo, and J. Sanz, J. Phys.: Condens. Matter **8**, 5355 (1996).
[15] L. Hagman and P. Kierkegaard, Acta Chem. Scand. **22**, 1822 (1968).
[16] J. B. Goodenough, H. Y. Hong, and J. A. Kafalas, Mater. Res. Bull. **11**, 203 (1976).
[17] H. Y. Hong, Mater. Res. Bull. **11**, 173 (1976).
[18] J. Angenault, C. Couturier, J. P. Souron, D. Siliqi, and M. Quarton, J. Mater. Sci. Lett. **11**, 1705 (1992).
[19] A. Martínez-Juárez, J. M. Rojo, J. E. Iglesias, J. Sanz, and R. Rojas, Chem. Mater. **6**, 1790 (1994).
[20] M. A. París, A. Martínez-Juárez, J. E. Iglesias, J. M. Rojo, and J. Sanz, Chem. Mater. **9**, 1430 (1997).
[21] F. Sudreau, D. Petit, and J. P. Boilot, J. Solid State Chem. **83**, 78 (1989).
[22] E. R. Losilla, M. A. G. Aranda, M. Martínez-Lara, and S. Bruque, Chem. Mater. **9**, 1678 (1997).
[23] J. E. Iglesias, J. Sanz, A. Martínez-Juárez, and J. M. Rojo, J. Solid State Chem. **130**, 322 (1997).
[24] J. E. Iglesias and C. Pecharromán, Solid State Ionics **112**, 309 (1998).
[25] M. A. París and J. Sanz, Phys. Rev. B **55**, 14 270 (1997).
[26] D. Massiot, WINFIT programme, ©Bruker-Franzen Analytik GmbH, 1993.
[27] J. Herzfeld and E. J. Berger, Chem. Phys. **73**, 6021 (1980).
[28] A. Abragam, *The Principles of Nuclear Magnetism* (Oxford University Press, Oxford, 1961).
[29] G. Engelhardt and D. Michel, *High Resolution Solid-State NMR of Silicates and Zeolites* (Wiley, New York, 1987).
[30] S. Ghose and T. Tsang, Am. Mineral. **58**, 748 (1973).
[31] D. Tran Qui, S. Hamdoune, and J. L. Soubeyroux, J. Solid State Chem. **72**, 309 (1988).
[32] M. Alami, R. Brochu, J. L. Souberyroux, P. Gravereau, G. Le Flem, and P. Hagenmuller, J. Solid State Chem. **90**, 185 (1991).
[33] E. Morin, J. Angenault, J. C. Couturier, M. Quarton, H. He, and J. Klinowski, Eur. J. Solid State Inorg. Chem. **34**, 947 (1997).
[34] M. Catti, S. Stramare, and R. Ibberson, Solid State Ionics **123**, 73 (1999).
[35] J. H. Van Vleck, Phys. Rev. **74**, 1168 (1948).
[36] R. M. Sternheimer, Phys. Rev. **84**, 244 (1951).
[37] R. M. Sternheimer, Phys. Rev. **86**, 316 (1952).
[38] R. M. Sternheimer, Phys. Rev. **146**, 140 (1966).
[39] E. A. C. Lucken, *Nuclear Quadrupole Coupling Constants* (Academic, London, 1969).
[40] A. Martínez-Juárez, C. Pecharromán, J. E. Iglesias, and J. M. Rojo, J. Phys. Chem. B **102**, 372 (1998).
[41] E. R. Losilla, M. A. G. Aranda, S. Bruque, M. A. París, J. Sanz, and A. R. West, Chem. Mater. **10**, 665 (1998).
[42] H. Kholer and H. Schulz, Mater. Res. Bull. **21**, 23 (1988).